Gaussian Process Sampling and Optimization with Approximate Upper and Lower Bounds

Vu Nguyen¹ Marc Peter Deisenroth² Michael A. Osborne³

Abstract

Many functions have approximately-known upper and/or lower bounds, potentially aiding the modeling of such functions. In this paper, we introduce Gaussian process models for functions where such bounds are (approximately) known. More specifically, we propose the *first* use of such bounds to improve Gaussian process (GP) posterior sampling and Bayesian optimization (BO). That is, we transform a GP model satisfying the given bounds, and then sample and weight functions from its posterior. To further exploit these bounds in BO settings, we present bounded entropy search (BES) to select the point gaining the most information about the underlying function, estimated by the GP samples, while satisfying the output constraints. We characterize the sample variance bounds and show that the decision made by BES is explainable. Our proposed approach is conceptually straightforward and can be used as a plugin extension to existing methods for GP posterior sampling and Bayesian optimization.

1. Introduction

Gaussian processes (GPs) provide a powerful probabilistic learning framework that has led to great success in many machine learning settings, such as black-box optimization (Brochu et al., 2010), reinforcement learning (Deisenroth & Rasmussen, 2011), hyperparameter tuning (Perrone et al., 2019; Parker-Holder et al., 2020), and battery forecasting (Richardson et al., 2017). GPs have been especially impactful for Bayesian optimization (BO) (Shahriari et al., 2016) to optimize a black-box function $f(\cdot)$, where careful uncertainty representation is crucial. A fundamental challenge for Gaussian process modeling and optimization is that data is often limited. In BO, a datum is usually an expensive evaluation of another model. Particularly, we evaluate and

Preprint. Copyright 2022 by the author(s).

optimize the underlying black-box without knowing the gradient or the analytical form of $f(\cdot)$. In the small data regime, it is always useful to utilize external knowledge about $f(\cdot)$, which has been successfully demonstrated in recent work, such as monotonicity trends (Riihimäki & Vehtari, 2010), experimenter's hunches (Li et al., 2018), and known optimum values (Nguyen & Osborne, 2020).

We propose to use another form of prior knowledge for improving both the GP posterior sampling and Bayesian optimization. We consider the maximum and minimum values of $f(\cdot)$. These optimal values can be found in machine learning applications, including inverse problems (Mosegaard & Tarantola, 1995; Aster et al., 2018; Bertero & Boccacci, 2020), where the goal is to retrieve an input \mathbf{x}^* resulting in the given target from a black-box function. Another example is tuning hyperparameters for classification algorithms (Krizhevsky et al., 2012); users may have vague knowledge about $f^+ := \max f(\cdot)$ and $f^- := \min f(\cdot)$, either from recent state-of-the-art results or directly from the definition of the accuracy metric $f^+ = 100\%$, $f^- = 0\%$. Similar information can be found in tuning regression problems where the best root mean square error (RMSE) score is known to be 0. Other examples are discussed by Nguyen & Osborne (2020), such as known maximum rewards for some reinforcement learning environments. Despite the usefulness of such prior knowledge for the low-data regime, the setting we consider in this paper, with *approximately known* maximum and minimum values, is new to the best of our knowledge.

In this paper, we propose to exploit the knowledge of maximum and minimum values of the black-box for improving the performance of GP posterior sampling and making better decisions in BO, especially when the number of observation is limited. Rather than using a regular GP as a surrogate model to infer the underlying function $f(\cdot)$, we transform the surrogate given the bound information. We assign different credits to samples based on the bounds and thus discard those falling outside. Moreover, we utilize these bounds for BO by proposing bounded entropy search (BES) to select the next point as that yielding the most information about the true underlying function. Our key contributions are:

the first use of exploiting knowledge about *both* the maximum f⁺ and/or minimum f⁻ values of a black-

¹Amazon Adelaide ²University College London ³University of Oxford. Correspondence to: Vu Nguyen <vu@ieee.org>.

box function, which can be approximately defined,

- an efficient posterior sampling procedure for f(·) that explicitly accounts for f⁺ and f[−],
- a bounded entropy search (BES) acquisition function for BO given f^+ and f^- .

2. Preliminaries

A black-box $f(\cdot)$ is defined over some bounded domain $\mathscr{X} \subset \mathbb{R}^d$ where *d* is the input dimension. The function *f* can only be accessed through noisy queries of the form $y_i \sim \mathscr{N}(f(\mathbf{x}_i), \sigma_f^2)$ where the input $\mathbf{x}_i \in \mathbb{R}^d$, the output $y_i \in \mathbb{R}$, and σ_f^2 is the output noise variance. We denote $\mathbf{X} = [\mathbf{x}_1, ..., \mathbf{x}_N]^T \in \mathbb{R}^{N \times d}$, $\mathbf{y} = [y_1, ..., y_N]^T \in \mathbb{R}^{N \times 1}$, and the training set at iteration *t* by $D_t = \{\mathbf{x}_i, y_i\}_{i=1}^t$.

2.1. Gaussian processes

We assume f to be drawn from a GP (Rasmussen & Williams, 2006) which is a random function $f : \mathscr{X} \to \mathbb{R}$, such that every finite collection of those random variables $f(\mathbf{X}_*) | \mathbf{X}_* \in \mathscr{X}$ follows a multivariate Gaussian distribution. Formally, we denote a GP as $f(\mathbf{x}) \sim \text{GP}(m(\mathbf{x}), k(\mathbf{x}, \mathbf{x}'))$, where $m(\mathbf{x}) = \mathbb{E}[f(\mathbf{x})]$ and $k(\mathbf{x}, \mathbf{x}') = \mathbb{E}\left[(f(\mathbf{x}) - m(\mathbf{x}))^T(f(\mathbf{x}') - m(\mathbf{x}'))\right]$ are the mean and covariance functions. Given the observed input \mathbf{X} and output \mathbf{y} , the GP posterior at a new input \mathbf{x}_* is defined as $f_* | \mathbf{X}, \mathbf{y}, \mathbf{x}_* \sim \mathcal{N}(\mu(\mathbf{x}_*), \sigma^2(\mathbf{x}_*))$. The posterior predictive mean and variance are given by

$$\boldsymbol{\mu}\left(\mathbf{x}_{*}\right) = \mathbf{k}_{*}^{T} \left[\mathbf{K} + \sigma_{f}^{2} \mathbf{I}\right]^{-1} \left(\mathbf{y} - \mathbf{m}\right) + m(\mathbf{x}_{*}) \qquad (1)$$

$$\sigma^{2}(\mathbf{x}_{*}) = k_{**} - \mathbf{k}_{*}^{T} \left[\mathbf{K} + \sigma_{f}^{2} \mathbf{I} \right]^{-1} \mathbf{k}_{*}$$
(2)

where $k_{**} = k(\mathbf{x}_*, \mathbf{x}_*)$, $\mathbf{k}_* = [k(\mathbf{x}_*, \mathbf{x}_i)]_{\forall i}^T \in \mathbb{R}^{N \times 1}$, $\mathbf{m} = [m(\mathbf{x}_i)]_{\forall i}^T \in \mathbb{R}^{N \times 1}$ and $\mathbf{K} = [k(\mathbf{x}_i, \mathbf{x}_j)]_{\forall i, j} \in \mathbb{R}^{N \times N}$.

Samples $g(\cdot) \sim GP(\mu(\cdot), \sigma^2(\cdot))$ from a GP posterior can be used for several applications, e.g., Thompson sampling (TS) (Thompson, 1933; Russo et al., 2018), or an informationtheoretic decision in BO (Hernández-Lobato et al., 2014; 2017; Kirthevasan et al., 2018). We follow the decoupled approach (Wilson et al., 2020; 2021) to draw samples $g(\cdot)$ from a GP posterior. The central idea of decoupled sampling relies on Matheron's rule for Gaussian random variables (Journel & Huijbregts, 1978; Chiles & Delfiner, 2009; Doucet, 2010), using variational Fourier features for an approximate prior and a deterministic data-dependent update term. The key benefit of this sampling is that the complexity scales linearly in the number of test points. This is particularly useful in optimizing the acquisition function in BO where we need to evaluate at many test points to select a next query (Wilson et al., 2018).

2.2. Optimum values prior in Bayesian optimization

BO aims at maximizing an expensive black-box function $f(\cdot)$ using few function evaluations, i.e. finding $\mathbf{x}^* := \arg \max_{\mathbf{x} \in \mathscr{X}} f(\mathbf{x})$. In BO, we typically construct a surrogate model of f using a GP. The surrogate model mimics the behavior of f while it is cheaper to evaluate. Then, we sequentially select points \mathbf{x}_t at which to evaluate f.

Prior knowledge about the optimum value of the blackbox contains useful information dictating the upper bound of $f(\cdot)$. A recent approach has considered the BO setting where the true optimum value $f^+ = \max_{\mathbf{x} \in \mathscr{X}} f(\mathbf{x})$ of the black-box function is available (Nguyen & Osborne, 2020). In particular, they transform the GP surrogate to satisfy that f^+ is an upper bound, and propose expected regret minimization (ERM) and confidence bound minimization (CBM) acquisition functions. However, this approach can be ineffective when the value of the true optimum max $f(\cdot)$ is not known. If the optimum value is mis-specified, the performance degrades. In addition, this approach can only cope with knowledge of f^+ , but it is unable to account for knowledge of both f^+ and f^- at the same time. The method we propose in this paper will overcome these limitations.

3. Gaussian process posterior sampling with approximate bounds f^+ and f^-

We consider settings where users know approximately the maximum and/or minimum value of f.

Definition 1. Define the approximate bounds as random variables: $f^+ \sim \mathcal{N}(\max f, \eta^2_+)$ and $f^- \sim \mathcal{N}(\min f, \eta^2_-)$.

We let users observe the realizations of the random variables f^+ and f^- , but not the means max f and min f. In these definitions, η_+ and η_- control the mis-specified levels or how loosely we define such bounds. We may observe both f^+ and f^- or either of them. The useful information f^+ and f^- give us is that (i) $f(\cdot)$ should not exceed these thresholds and (ii) $f(\cdot)$ should attain closely f^+, f^- . In particular, for maximization problems, the location at which f^+ is attained, is *potentially* the global maximizer of f we are looking for in BO settings.

3.1. Sampling and weighting GP posterior samples

Although the existing GP posterior sampling approach (Wilson et al., 2020) has demonstrated great success, the resulting GP samples usually do not obey the bounds $[f^-, f^+]$. Intuitively, assume we are given a few (noisy) observations from the black-box f. We can be confident in deciding which GP samples are not admissible by looking at the bounds f^+, f^- and thus not making use of these samples. Therefore, we propose to assign different credits to the GP samples based on the bound knowledge.

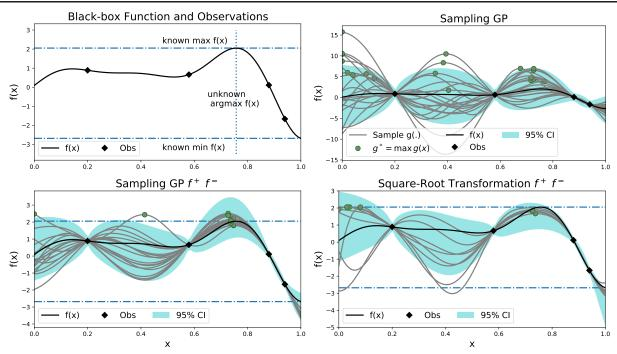


Figure 1: *Top Right*: Decoupled GP sampling (Wilson et al., 2020) given four observations from $f(\mathbf{x})$. *Bottom Left*: GP sampling and weighting with both f^+ and f^- . *Bottom Right*: GP sampling and weighting with square-root transformation (or square-root transformed Gaussian process (SRGP). Given limited observations, the existing GP sampling can be misleading to fluctuate widely beyond the bounds (see the *y-axis*) while exploiting f^+ and f^- can result in better GP sample.

The GP sample evaluated at any location **x** can be written as $\hat{g}(\mathbf{x}) := \mathbb{E}\left[p(f \mid \mathbf{X}, \mathbf{y}, f^+, f^-)\right]$ which is marginalized across all GP samples as:

$$\hat{g}(\mathbf{x}) = \int_{g(\cdot)} p\Big(f(\mathbf{x}) \mid \mathbf{x}, g(\cdot)\Big) p\Big(g(\cdot) \mid \mathbf{X}, \mathbf{y}, f^+, f^-\Big) dg(\cdot)$$
$$\approx \sum_{g_m(\cdot) \sim p_{\text{base}}} g_m(\mathbf{x}) \pi(g_m). \tag{3}$$

where p_{base} denotes the base distribution to generate GP posterior samples (e.g., using decoupling approach (Wilson et al., 2020)). $g_m(\mathbf{x})$ is the value at location \mathbf{x} from a GP sample g_m , see Eq. (13) in the appendix for details. We denote $\pi(g_m) := p(g_m(\cdot) | \mathbf{X}, \mathbf{y}, f^+, f^-)$ which assigns high probability to a sample g_m satisfying the approximate bounds while it assigns zero or very low probability otherwise. We define $\pi(g_m)$ in the next section.

3.2. The weighting probability $\pi(g_m)$ given f^+ and f^-

Given the data \mathbf{X}, \mathbf{y} , we draw M samples from a GP and expect that a GP sample $g_m(\cdot)$ naturally follows the conditions: (i) $f^- \leq g_m(\cdot) \leq f^+$ and (ii) $\exists \mathbf{x}_m^+$ such that $g_m(\mathbf{x}_m^+) \approx f^+$ and $\exists \mathbf{x}^-$ such that $g_m(\mathbf{x}^-) \approx f^-$. Let us denote the maximum and minimum values of the sample by $g_m^+ = \max g_m(\cdot)$ and $g_m^- = \min g_m(\cdot)$, respectively. To satisfy the above conditions, we define the weighting probability $\pi(g_m)$ using an isotropic bivariate Gaussian distribution:

$$\pi(g_m) := \mathscr{N}\left(\left[g_m^-, g_m^+\right] \mid \left[f^-, f^+\right], \operatorname{diag}[\eta_-^2, \eta_+^2]\right). \quad (4)$$

The mean of $\pi(g_m)$ is located at $[f^-, f^+]$ and the *M* observations are $[g_m^-, g_m^+], m = 1, ..., M$ which are the min and max values of the GP posterior samples, see Fig. 2 (left). This bivariate will flexibly collapse into a univariate Gaussian when either f^+ or f^- is observed.

The view of rejection sampling. The weighting scheme above can be seen from the rejection-sampling perspective. We accept a GP sample $g_m(\cdot)$ if it lies within a two standard deviation band around the mean of $\pi(g_m)$ as illustrated in Fig. 2 (right). Specifying a smaller value for η_+ will make $\pi(g_m)$ strict and only accept a GP sample which has the maximum value max $g_m(\cdot)$ closer to f^+ . On the other hand, increasing η_+, η_- will lead to more accepted samples, but in lower quality. We visualize $\pi(g_m)$ using different values of $\eta = \{1, 2\}$ in Fig. 2 (right). We have simplified the two-dimensional space into one dimension for better representation.

3.3. Square-root GP for sampling g_m

We utilize Matheron's rule to efficiently draw samples from a GP through p_{base} . However, taking a standard GP model for p_{base} can lead to unwanted samples being taken, as

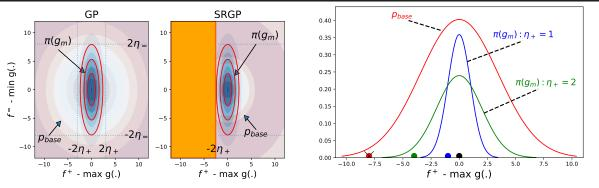


Figure 2: Illustration of the sampling and weighting step. Left: We can use a GP or a SRGP for p_{base} . Given the same weighting probability $\pi(g_m)$, using SRGP has a smaller sample variance by ignoring the redundant space (orange area). Right: For ease of representation, we use a univariate Gaussian distribution to visualize $\pi(g_m)$. The GP sample $g_m(\cdot)$ (represented by the maximum value of $g_m(\cdot)$ is drawn from p_{base} . We assign high weight to a sample depending on the density of $\pi(g_m)$. The red point will be rejected. The green point falls within the density of $\pi(g_m)$ with $\eta_+ = 2$, but not for $\eta_+ = 1$. The blue point receives positive weights by both $\pi(g_m)$ including $\eta_+ = 1$ and $\eta_+ = 2$. The **black** point receives the highest weight.

Table 1: Acceptance ratio over M = 200 samples from p_{base} as a GP and a SRGP respectively. See Section 5 for detail.

	$\eta_+=\eta$	$_{-} = 0.5d$	$\mid \eta_+ = \eta$	$\eta_+ = \eta = 1d$			
	GP	SRGP	GP	SRGP			
branin d=2	.39(.2)	. 89 (. 2)	.62(.1)	. 96 (. 2)			
rosenbrock d=2	.52(.2)	. 88 (. 2)	.62(.2)	.95(.2)			
mccormick d=2	.65(.1)	. 91 (. 2)	.69(.1)	1.0(.1)			
hartmann d=3	.08(.1)	.40(.3)	.31(.2)	.76(.2)			
alpine1 d=5	.0(.0)	.13(.1)	.10(.1)	.30(.2)			
gSobol d=5	.01(.1)	.46(.3)	.14(.2)	.74(.4)			

demonstrated empirically in Table 1 especially for highdimensional functions such as *alpine1* and *gSobol*. Here, we consider a sample is accepted when the density of $\pi(g_m)$ is within two standard deviation of the Gaussian distribution defined in Eq. (4) and rejected otherwise.

Therefore, we propose to use a transformed GP surrogate model given f^+ for p_{base} , using a technique presented by Gunter et al. (2014). Based on Definition 1, we have that $f^+ \in \left[\max f(\mathbf{x}) - 2\eta_+, \max f(\mathbf{x}) + 2\eta_+\right]^1$ with high probability. Therefore, we can write $\forall \mathbf{x}, f(\mathbf{x}) \leq f^+ + 2\eta_+$. Thus, there exists $h(\cdot)$ satisfying $\forall \mathbf{x}, f(\mathbf{x}) = f^+ + 2\eta_+ - h^2(\mathbf{x})$. Formally, we define $f(\cdot)$ via $h(\cdot) \sim GP$ as follows:

$$f(\cdot) = f^+ + 2\eta_+ - \frac{1}{2}h^2(\cdot), \text{ where } h \sim \operatorname{GP}(m_h, K_h).$$
 (5)

This transformation ensures the resulting function $f(\cdot)$ to satis fy the bounded constraints $f^+ \gtrsim f(\cdot)$ and $\exists \mathbf{x}^+, f(\mathbf{x}^+) \rightarrow$ f^+ when $h(\mathbf{x}^+) \rightarrow 0$. We refer to Fig. 1 (bottom right) for an illustration of this transformation.

We estimate a posterior for drawing samples of $h(\cdot)$

Algorithm 1 SRGP-weighting with f^+, f^-

- 1: **Input:** #GP sample M, data D, f^+ , f^-
- 2: Learn a SRGP posterior model \mathscr{G} from D and f^+
- 3: Draw GP samples g_1, \dots, g_M from p_{base} by (i) drawing from $\mu_h(\cdot)$ and (ii) computing $\mu_f(\cdot)$ in Eq. (6)
- 4: Compute $\pi(g_m), \forall m = 1, ..., M$ by Eq. (4) 5: **Output:** $\hat{g}(\mathbf{x}) = \sum_{m=1}^{M} g_m(\mathbf{x}) \pi(g_m)$

as follows. Denote the data in the original space by $D_f = \{\mathbf{x}_i, y_i\}_{i=1}^N \text{ where } y_i \leq f^+ + 2\eta_+, \text{ we compute } D_h = \{\mathbf{x}_i, h_i\}_{i=1}^N \text{ where } h_i = \sqrt{2(f^+ + 2\eta_+ - y_i)}. \text{ Next we write the posterior of } p(h(\mathbf{x}_*) \mid D_h) \approx \mathscr{N}(\mu_h(\mathbf{x}_*), \sigma_h^2(\mathbf{x}_*)) \text{ with }$ $\mu_h(\mathbf{x}_*) = m_h(\mathbf{x}_*) + \mathbf{k}_*^T \left[\mathbf{K} + \sigma_h^2 \mathbf{I} \right]^{-1} (h - m_h) \text{ and } \sigma^2(\mathbf{x}_*) =$ $k_{**} - \mathbf{k}_{*}^{T} \left[\mathbf{K} + \sigma_{h}^{2} \mathbf{I} \right]^{-1} \mathbf{k}_{*}$ where σ_{h}^{2} is the measurement noise variance of $h(\cdot)$ and other variables are defined analogously to Section 2.1.

We draw GP samples from $h(\cdot)$ to get $f(\cdot)$ using Eq. (5). The resulting samples of $f(\cdot)$ follow the upper bound conditions as desired—staying below f^+ and reaching (closely) the optimum value. After using f^+ to sample $f(\cdot)$, we further exploit f^- via the weighting scheme using Eq. (4).

To estimate the posterior predictive mean and variance in the original space, we use a Taylor expansion to approximate the posterior predictive distribution (Gunter et al., 2014) $p(f(\mathbf{x}_*) | \mathbf{X}, \mathbf{y}, \boldsymbol{\eta}_+, f^+) \approx \mathcal{N}(\boldsymbol{\mu}_f, \boldsymbol{\sigma}_f^2)$ where

$$\mu_f(\mathbf{x}_*) = f^+ + 2\eta_+ - \frac{1}{2}\mu_h^2(\mathbf{x}_*)$$
(6)

$$\sigma_f^2(\mathbf{x}_*) = \mu_h^2(\mathbf{x}_*)\sigma_h^2(\mathbf{x}_*)\mu_h^2(\mathbf{x}_*).$$
(7)

We will use these two expressions for computing the acquisition function presented in Section 4. We summarize the above process in Algorithm 1.

 $^{{}^{1}2\}eta_{+}$ is chosen to cover 95% of the probability density

3.4. Tightening the variances of GP posterior samples

The base distribution p_{base} for drawing GP posterior samples in Eq. (3) can be used as (i) standard GP (Wilson et al., 2020), (ii) weighting using GP or (iii) weighting using SRGP (presented in Section 3.3), respectively. For brevity, we denote these approaches as p_{GP} , $p_{\text{w-GP}}$ and $p_{\text{w-SRGP}}$.

We show that our approaches p_{W-GP} and p_{W-SRGP} will tighten the sample variance relative to p_{GP} ignoring the bounds f^+ , f^- . We state the main theoretical results and refer to Appendix A.3 for the proofs.

Lemma 1. In the 2d space formed by $[f^+, f^-]$ and the GP posterior samples $\{g_m^+, g_m^-\}_{m=1}^M$, the sample variances by weighting SRGP and GP are smaller than the GP posterior sampling (Wilson et al., 2020) making no use of the bounds: $Var[p_{W-GP}] \leq Var[p_{GP}]$ and $Var[p_{W-SRGP}] \leq Var[p_{GP}]$.

To intuitively understand our analysis, we visualize these variances in the 2d space in Fig. 2 (left), created by $[f^+, f^-]$ and $\{g_m^+, g_m^-\}_{m=1}^M$ taken from GP posterior samples. In Lemma 1, the sample variances using our approaches will be smaller than the approach in (Wilson et al., 2020), which makes no use of the bounds. This highlights the benefit of using the bounds to eliminate bad samples, which violate the bounds, to obtain a smaller sample variance.

Next, we show in Lemma 2 that using $p_{\text{w-SRGP}}$ will be more sample-efficient than using $p_{\text{w-GP}}$. In other words, we get more accepted samples by using the weighting SRGP, given the same number of posterior samples M.

Lemma 2. In the 2d space formed by $[f^+, f^-]$ and the GP posterior samples $\{g_m^+, g_m^-\}_{m=1}^M$, the sample variance of weighting SRGP is smaller than weighting GP: $Var[p_{w-SRGP}] \leq Var[p_{w-GP}].$

4. Bounded entropy search for Bayesian optimization given f^+ and f^-

The knowledge of f^+ and f^- is also applicable and useful to inform and speed up BO. Given a collection of GP samples representing the underlying function $f(\cdot)$, each satisfies the bounds at different degrees. For BO setting, we can not take all of them, but to select a single point for evaluation among these M candidates. We derive an acquisition function to find a single point maximizing the information gain about 'good' GP posterior samples satisfying the bounds.

Bounded entropy search (BES). Let us write $\mathbf{x}_m^+ := \arg \max_{\mathbf{x}} g_m(\mathbf{x})$ as the maximum location of the *m*-th sample from a GP posterior and $g_m^+ = \max g_m(\mathbf{x}) = g_m(\mathbf{x}_m^+), m = 1, ..., M$ be the corresponding maximum value. We propose to select a next point $\mathbf{x}_t := \arg \max_{\mathbf{x} \in \mathscr{X}} \alpha^{\text{BES}}(\mathbf{x})$ by maximizing the mutual information given the optimum samples

Algorithm 2 BO with BES given f^+, f^- 1: Input: #iter T, data D_0, f^+, f^-

2: for t = 1, ..., T do

- 3: Draw GP samples g_1, \ldots, g_M given D_{t-1}
- 4: $\mathbf{x}_t = \arg \max \alpha^{\text{BES}}(\mathbf{x} \mid g_1, ..., g_M)$ by Eq. (9)
- 5: Evaluate $y_t = f(\mathbf{x}_t)$ and $D_t = D_{t-1} \cup (\mathbf{x}_t, y_t)$

7: **Output:** $\arg \max_{\mathbf{x} \in \mathscr{X}} \mu_T(\mathbf{x} \mid D_T)$

 $\{g_m^+, \mathbf{x}_m^+\}$ and f^+, f^- , i.e.,

$$\boldsymbol{\alpha}^{\text{BES}}(\mathbf{x}) := I\left(y_{\mathbf{x}}, \{g_m^+, \mathbf{x}_m^+\} \mid \mathbf{X}, \mathbf{y}, f^+, f^-\right).$$
(8)

Our acquisition function aims at gaining the most information about the GP posterior samples $g_m(\cdot)$. Equivalently it learns the most about $f(\cdot)$, especially at the locations giving the outputs closer to the known optimum values f^+ . Although the idea of gaining information about the optimums has been extensively used in recent works (Hennig & Schuler, 2012; Hernández-Lobato et al., 2014; Wang & Jegelka, 2017), we are *the first* to extend it to situations when the knowledge about f^+ and f^- is available.

Denote $y_{\mathbf{x}} := \mathbb{E}[f_{\mathbf{x}} | \mathbf{X}, \mathbf{y}, \mathbf{x}], \ \Upsilon_m = \{g_m^+, \mathbf{x}_m^+\} \text{ and } \Lambda := \{\mathbf{X}, \mathbf{y}, f^+, f^-\} \text{ for brevity, we can write the mutual information using the KL divergence as } I(y_{\mathbf{x}}, \Upsilon_m | \Lambda)$

$$\approx \frac{1}{M} \sum_{\Upsilon_m \sim p_{\text{base}}} \int p(\Upsilon_m, y_{\mathbf{x}} \mid \Lambda) \log \frac{p(y_{\mathbf{x}}, \Upsilon_m \mid \Lambda)}{p(y_{\mathbf{x}} \mid \Lambda) p(\Upsilon_m \mid \Lambda)} dy_{\mathbf{x}}$$
$$= \frac{1}{M} \mathbb{E}_{p(y_{\mathbf{x}} \mid \Lambda)} \left[\sum_{\Upsilon_m \sim p_{\text{base}}} p(\Upsilon_m \mid y_{\mathbf{x}}, \Lambda) \log \frac{p(\Upsilon_m \mid y_{\mathbf{x}}, \Lambda)}{p(\Upsilon_m \mid \Lambda)} \right]$$
(9)

where $\Upsilon_m = \{g_m^+, \mathbf{x}_m^+\} \sim p_{\text{base}}$ is generated as follows: $g_m \sim p_{\text{base}}$, $\mathbf{x}_m^+ = \arg \max g_m(\cdot)$, $g_m^+ = g_m(\mathbf{x}_m^+)$ and $y_{\mathbf{x}} \approx g_m(\mathbf{x})$. We have used the product rule $p(y_{\mathbf{x}}, g_m^+, \mathbf{x}_m^+ \mid \Lambda) = p(y_{\mathbf{x}} \mid \Lambda) p(g_m^+, \mathbf{x}_m^+ \mid y_{\mathbf{x}}, \Lambda)$ to simplify the terms.

Given $\pi(g_m) = \mathcal{N}([g_m^-, g_m^+] | [f^-, f^+], \operatorname{diag}[\eta_-^2, \eta_+^2])$ in Eq. (4), we want to quantify the influence of a new data point {**x**, *y*_{**x**}} on a given GP posterior sample. We write the probability with and without the presence of **x**

$$p\left(g_{m}^{+}, \mathbf{x}_{m}^{+} \mid \Lambda\right) = p\left(g_{m}^{+} \mid \mathbf{x}_{m}^{+}, \Lambda\right) p\left(\mathbf{x}_{m}^{+} \mid \Lambda\right)$$
(10)
$$= \pi(g_{m}) \mathcal{N}\left(g_{m}^{+} \mid \mu(\mathbf{x}_{m}^{+}), \sigma^{2}(\mathbf{x}_{m}^{+})\right)$$

$$p\left(g_{m}^{+}, \mathbf{x}_{m}^{+} \mid \mathbf{y}_{\mathbf{x}}, \Lambda\right) = p\left(g_{m}^{+} \mid \mathbf{x}_{m}^{+}, \mathbf{y}_{\mathbf{x}}, \Lambda\right) p\left(\mathbf{x}_{m}^{+} \mid \mathbf{y}_{\mathbf{x}}, \Lambda\right)$$
(11)
$$= \pi(g_{m}) \mathcal{N}\left(g_{m}^{+} \mid \boldsymbol{\mu}_{\mathbf{x}}(\mathbf{x}_{m}^{+}), \sigma_{\mathbf{x}}^{2}(\mathbf{x}_{m}^{+})\right)$$

where $\mu_{\mathbf{x}}(\mathbf{x}_m^+)$, $\mu(\mathbf{x}_m^+)$, $\sigma_{\mathbf{x}}^2(\mathbf{x}_m^+)$, and $\sigma^2(\mathbf{x}_m^+)^2$ are the GP posterior predictive means and variances at \mathbf{x}_m^+ with and without the inclusion of \mathbf{x} . These predictive quantities are

²we use subscript $\sigma_{\mathbf{x}}(\cdot)$ to indicate the inclusion of \mathbf{x} while $\sigma(\cdot)$ is without \mathbf{x} .

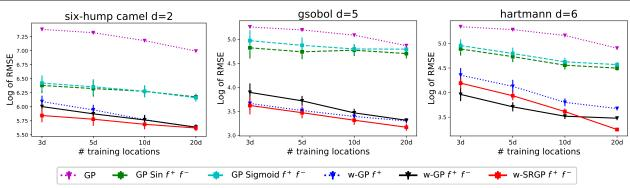


Figure 3: Exploiting the external knowledge about f^+ and f^- will lead to better GP posterior sampling.

defined in Eqs. (6) and (7). Plugging Eqs. (10) and (11) into Eq. (9), we obtain the final form of $\alpha^{\text{BES}}(\mathbf{x})$.

Without knowing the true output at a test location \mathbf{x} , we can simplify the GP predictive mean $\mu_{\mathbf{x}}(\mathbf{x}_m^+) \approx \mu(\mathbf{x}_m^+)$. This simplification saves computation cost for updating the GP predictive mean at each considered location \mathbf{x} .

The term $\pi(g_m)$ in Eq. (11) will be retained when plugging into Eq. (9). Thus, $\pi(g_m)$ will cancel out any GP sample which does not follow our bounded constraints. As a result, our decision only gains information about the 'good' samples, weighted by how likely it is. In Appendix C.4, we provide an ablation study by accepting all samples (without weighting step), which drops the performance significantly.

Explainable decision. The point selected by Eq. (9) will gain the maximum information about the posterior samples. Our decision can be interpretable in each single term. The acquisition function value in Eq. (9) is high when the density $\frac{p(g_m^+, \mathbf{x}_m^+ | \mathbf{y}_{\mathbf{x}}, \Lambda)}{p(g_m^+, \mathbf{x}_m^+ | \Lambda)}$ and $p(g_m^+, \mathbf{x}_m^+ | \mathbf{y}_{\mathbf{x}}, \Lambda)$ are high, defined in Eqs. (10) and (11). The first term $\frac{p(g_m^+, \mathbf{x}_m^+ | \mathbf{y}_{\mathbf{x}}, \Lambda)}{p(g_m^+, \mathbf{x}_m^+ | \Lambda)} \propto$ $\mathscr{N}(g_m^+ \mid \boldsymbol{\mu}(\mathbf{x}_m^+), \left[\boldsymbol{\sigma}_{\mathbf{x}}^2(\mathbf{x}_m^+)^{-1} - \boldsymbol{\sigma}^2(\mathbf{x}_m^+)^{-1}\right]^{-1}) \text{ is high when}$ $\sigma_{\mathbf{x}}^2(\mathbf{x}_m^+) \ll \sigma^2(\mathbf{x}_m^+)$ given that $\mathbb{E}[g_m^+] = \mu(\mathbf{x}_m^+)$. To reduce this predictive uncertainty of $\sigma_x^2(\mathbf{x}_m)$, our acquisition function encourages to place a point \mathbf{x} at the perceived optimum location \mathbf{x}_m^+ . Similarly, the second term $p(g_m^+, \mathbf{x}_m^+ | y_{\mathbf{x}}, \Lambda)$ takes high value when $\pi(g_m)$ is high and $\sigma_{\mathbf{x}}^2(\mathbf{x}_m^+)$ is small. This encourages (i) the sampled GP has the maximum value g_m^+ consistent with f^+ and (ii) taking a location at \mathbf{x}_m^+ . We refer to Appendix B for the illustration of the α^{BES} and A.2 for the implementation discussion. We summarize all steps for computing BES in Algorithm 2.

5. Experiments

We demonstrate the two claims in exploiting the knowledge of f^+ and f^- for improving GP posterior sampling and BO. We also perform ablation studies by varying the misspecified levels of such bounds for each setting. All experiments are averaged over 30 independent runs, the number of GP samples $M = 200,^3 \eta^2_+ = 0.02d$ and $\eta^2_- = 0.5d$ where *d* is the input dimension. The dimension of random Fourier feature is set to default as l = 100. We normalize the input $\mathbf{x} \in [0, 1]^d$ and standardize the output $y \sim \mathcal{N}(0, 1)$ for robustness. We follow the common practice in optimizing GP hyperparameter by maximizing the GP log marginal likelihood (Rasmussen & Williams, 2006). We refer to the appendix for additional experiments, illustrations, and ablation studies. We attach the Python source code in the submission and will release publicly in the final version.

SRGP vs GP. The key advantage of SRGP is that we can generate 'good' samples more often than using a standard GP in Section 3.1. We demonstrate this benefit in Fig. 2 showing that SRGP with weighting (or w-SRGP) outperforms w-GP. The results are more significant in higher dimensional functions where the w-GP cannot get a single sample accepted for *alpine1* in 5*d* using M = 200. In other words, the proposed w-SRGP will be more efficient to achieve the same number of accepted GP samples given f^+, f^- .

Improving GP posterior sampling. A set of training locations $\mathbf{X}_{\text{train}} \sim U[0, 1]^{N_{\text{train}} \times d}$ is randomly generated and corresponding outputs $\mathbf{y}_{\text{train}} = f(\mathbf{X}_{\text{train}})$ are subsequently observed. We construct a GP given $\{\mathbf{X}_{\text{train}}, \mathbf{y}_{\text{train}}\}$ and draw M = 200 GP posterior samples for each sampling scheme. Due to the trade-off between the number of accepted GP samples versus the sampling quality for these methods with exploiting f^+ and f^- , we rank and select the same (M' = 100) number posterior samples from the initial set of M = 200 samples above. These samples are used to compute the RMSE error against the true $f(\cdot)$.

We vary the number of training locations $N_{\text{train}} = \{3d, 5d, 10d, 20d\}$ and report the results in Fig. 3 which suggest that increasing the number of training observations will reduce the error for all sampling schemes. More importantly, incorporating the knowledge about f^+ and f^-

³The ablation study with different choices of $M \in \{20, 50, 200, 300, 500\}$ is available in Appendix C.1

Gaussian Process Sampling and Optimization with Approximate Upper and Lower Bounds

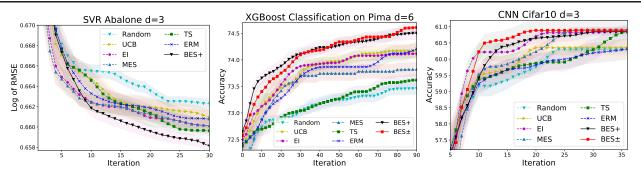


Figure 4: Machine learning hyperparameter tuning tasks. Exploiting the knowledge about optimum values will lead to better optimisation performance. BES \pm (with f^+ and f^-) performs the best. In SVR setting, we only use f^+ while we have ultilized both f^+ and f^- for XGBOOST and CNN.

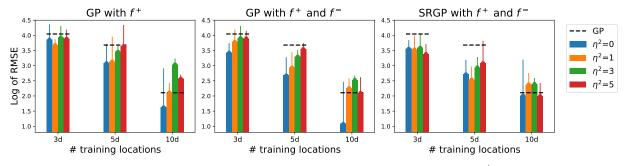


Figure 5: Our method can improve the performance of GP posterior sampling without using f^+ or f^- (Wilson et al., 2020) (black dash line) under misspecification of f^+ , f^- . The gap is more significant given fewer training observations. The plot is using Forrester function. See the Appendix Fig. 12 for more results.

will significantly improve the GP posterior sampling performance. Furthermore, using both f^+ and f^- results in better performance than using f^+ alone. Our approach surpasses the standard GP sampling (Wilson et al., 2020), which does not use the bound information, by a wide margin. The logistic and sigmoid transformations making use of the bounds are generally better than the standard GP, but are inferior to our proposed methods. We present further details and visualization of these transformations in Appendix A.1.

Improving Bayesian optimization. We next present a BO task. We follow a popular evaluation criteria in information theoretic approaches (Hennig & Schuler, 2012; Hernández-Lobato et al., 2014) that selects the inferred argmax of the function for evaluation, i.e. $\tilde{\mathbf{x}}_T =$ $\operatorname{arg} \max_{\mathbf{x} \in \mathscr{X}} \mu_T(\mathbf{x} \mid D_T)$. The number of BO iterations is 10*d*, initialized by *d* observations randomly where *d* is the number of input dimension. We compare our model with standard BO methods which do not use f^+ and f^- , including GP-UCB (Srinivas et al., 2010), expected improvement (EI) (Mockus et al., 1978), max-value entropy search (MES) (Wang & Jegelka, 2017) and Thompson sampling (TS). We compare with ERM (Nguyen & Osborne, 2020), which can make use of either f^+ or f^- , but not both of them. We compare the performance using popular benchmark functions and machine learning hyperparameter tunings including support vector regression (Smola & Vapnik, 1997) on Abalone, XGBOOST (Chen & Guestrin, 2016) classification on Pima Indians diabetes, and a CNN (LeCun & Bengio, 1995) on CIFAR10. We refer to Appendix C.4 for studying a variant of BES where $\pi(g_m) = \frac{1}{M}$ is set uniformly and Appendix D.2 for additional experiments.

BES \pm is an abbreviation for BES using both f^+ and $f^$ while BES+ uses f^+ alone. We show in Fig. 4 that exploiting the optimum knowledge in our BES and ERM should perform competitively. Notably, our BES often achieves high performances at the *earlier stage* of the optimization process where we do not have much information to infer the underlying function. Therefore, utilizing f^+ , f^- will bring significant benefits at the earlier stage that the existing approaches are unable to exploit. We note that when f^+ and f^- are available, the ERM is unable to exploit both.

Misspecifying f^+ and f^- . We perform ablation studies over different misspecified levels of the optimum values via $\eta^2 := \eta^2_+ = \eta^2_- \in \{0, 1, 3, 5\}$ for GP sampling and $\eta^2 \in \{0, 0.3, 0.5, 1\}$ for BO. Using the benchmark functions, we access to the true values of max $f(\cdot)$ and min $f(\cdot)$. Thus, the misspecified value is set as $f^+ = \max f(\cdot) \pm \eta^2_+$ where \pm is randomly selected by a Bernoulli random variable. f^- is specified analogously.

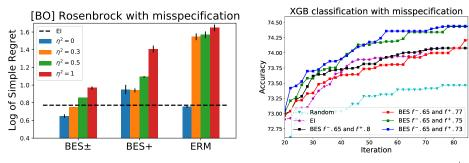


Figure 6: Left: our BES is more robust than ERM in dealing with misspecification. Right: We specify f^+ to different values and set f^- fixed in XGBOOST. The performance is better when f^+ is set closer to the true value ≈ 0.745 .

For a meaningful study, we consider these values after standardizing the output space $y \sim \mathcal{N}(0,1)$. This means that when $\eta^2 = 1$, the gap between the true max $f(\cdot)$ and the specified f^+ is one standard deviation of $f(\cdot)$. We present further experimental results in the Appendix Fig. 12.

When $\eta^2 \leq 1$, the performance of GP posterior sampling in Fig. 5 is much better than Wilson et al. (2020) in all cases and when $\eta^2 \leq 5$ our model is still better in a few cases. Relaxing $\eta^2 \rightarrow \infty$ will let the performance of w-GP reduce to the case of Wilson et al. (2020) while the performance of w-SRGP will slightly suffer because the transformation depends on η^2_+ . Thus, we suggest to use our weighting SRGP when the misspecification is such that $\eta^2 \leq 1$, one standard deviation of $f(\cdot)$, and use w-GP otherwise.

We study misspecifying f^+ and f^- for BO. In Fig. 6 (left), our BES performs competitively the best, especially when $\eta^2 \leq 0.3$ in all cases. The information gain strategy in BES is more noise-resilient in dealing with misspecification than ERM. Especially if we underspecify f^+ , the performance of ERM will significantly drop as shown in Nguyen & Osborne (2020), while our BES can tolerate better. Utilizing both information about f^+ and f^- will help to cope with misspecification better than using f^+ alone.

In Fig. 6 (right), we vary the values of f^+ within [0.7, 0.9] and fix $f^- = 0.65$ in the XGBOOST classification problem where we do not know the true value for these bounds. The result indicates that the best performance for BES is achieved when f^+ is set close to ≈ 0.745 , which is likely the true (but unknown) upper bound. Our BES with misspecifying $f^+ \in [0.73, 0.75]$ still performs generally better than EI.

6. Conclusion, limitations and future work

Conclusion. We have presented a new setting and approaches for exploiting the upper and lower bounds available for some black-box functions. We exploit these bounds for improving the performance of GP posterior sampling and BO. The resulting GP posterior sampling approach has tighter sample variance bounds than existing methods. Our approaches can be used as a plugin extension to existing

distributed and asynchronous Thompson sampling as well as sparse GP models.

Comparisons with ERM (Nguyen & Osborne, 2020). Our key advantages against ERM is as follows. First, our approach can handle the information about *both* the max and min of $f(\cdot)$ while the setting in ERM can only handle *one* of them. Second, our approach is more widely applicable in taking the optimum values which can be *loosely* specified while ERM expects to observe the *precise* value. Particularly, ERM will perform poorly if users underspecified the true value of max_x f(x). Third, our approach is useful for both GP posterior sampling and BO settings while the one suggested by Nguyen & Osborne (2020) is limited to BO.

Limitations. While we believe the results above are insightful, there are a number of limitations one should be aware of. First, our BES relies on the GP posterior samples to make a decision. There will be some iterations where none of the GP samples stays within the approximate bounds, such as when M is small or the available data is biased to represent $f(\cdot)$. Whenever this happens, our BES may be not applicable; instead we can simply perform EI (Jones et al., 1998) for this iteration. We found this simple trick with EI works well empirically and illustrate it in Appendix C.2. Second, we acknowledge the challenge when the bounds are heavily mis-specified, where such knowledge about the bounds can be less beneficial. Thus, the results in Fig. 6 suggest that if our loose bounds are defined more than $\eta^2 > 0.3$, it may be better to use existing acquisition functions, such as EI, without using the external knowledge.

Future work can extend the model to optimize multiple objectives simultaneously, each of which comes with loose upper and lower bounds. Using such bounds, other future works can be to improve parallel Thompson sampling (Hernández-Lobato et al., 2017; Kirthevasan et al., 2018) or used jointly with other signals, such as monotonicity, for the best performance in the low data regime. Another direction for improving the sample efficiency is to consider important sampling on the space of random Fourier feature while we expect the high dimensional challenge.

References

- Aster, R. C., Borchers, B., and Thurber, C. H. *Parameter Estimation and Inverse Problems*. Elsevier, 2018.
- Bertero, M. and Boccacci, P. Introduction to inverse problems in imaging. CRC press, 2020.
- Brochu, E., Cora, V. M., and De Freitas, N. A tutorial on Bayesian optimization of expensive cost functions, with application to active user modeling and hierarchical reinforcement learning. *arXiv preprint arXiv:1012.2599*, 2010.
- Chen, T. and Guestrin, C. Xgboost: A scalable tree boosting system. In *Proceedings of the 22nd ACM SigKDD International Conference on Knowledge Discovery and Data Mining*, pp. 785–794. ACM, 2016.
- Chiles, J.-P. and Delfiner, P. Geostatistics: Modeling Spatial Uncertainty, volume 497. John Wiley & Sons, 2009.
- Deisenroth, M. P. and Rasmussen, C. E. PILCO: a modelbased and data-efficient approach to policy search. In *Proceedings of the International Conference on Machine Learning*, pp. 465–472, 2011.
- Doucet, A. A note on efficient conditional simulation of Gaussian distributions. *Department of Computer Science and Statistics, University of British Columbia*, 4, 2010.
- Gunter, T., Osborne, M. A., Garnett, R., Hennig, P., and Roberts, S. J. Sampling for inference in probabilistic models with fast Bayesian quadrature. In *Advances in Neural Information Processing Systems*, pp. 2789–2797, 2014.
- Hennig, P. and Schuler, C. J. Entropy search for informationefficient global optimization. *Journal of Machine Learning Research*, 13:1809–1837, 2012.
- Hernández-Lobato, J. M., Hoffman, M. W., and Ghahramani, Z. Predictive entropy search for efficient global optimization of black-box functions. In Advances in Neural Information Processing Systems, pp. 918–926, 2014.
- Hernández-Lobato, J. M., Requeima, J., Pyzer-Knapp, E. O., and Aspuru-Guzik, A. Parallel and distributed Thompson sampling for large-scale accelerated exploration of chemical space. *In International Conference on Machine Learning*, pp. 1470–1479, 2017.
- Jones, D. R., Schonlau, M., and Welch, W. J. Efficient global optimization of expensive black-box functions. *Journal of Global Optimization*, 13(4):455–492, 1998.
- Journel, A. G. and Huijbregts, C. J. *Mining Geostatistics*, volume 600. Academic Press London, 1978.

- Kirthevasan, K., Akshay, K., Jeff, S., and Barnabas, P. Parallelised Bayesian optimisation via Thompson sampling. In AISTATS, 2018.
- Krizhevsky, A., Sutskever, I., and Hinton, G. E. Imagenet classification with deep convolutional neural networks. In Advances in Neural Information Processing Systems, pp. 1097–1105, 2012.
- LeCun, Y. and Bengio, Y. Convolutional networks for images, speech, and time series. *The handbook of brain theory and neural networks*, 3361(10):1995, 1995.
- Li, C., Santu, R., Gupta, S., Nguyen, V., Venkatesh, S., Sutti, A., Leal, D. R. D. C., Slezak, T., Height, M., Mohammed, M., and Gibson, I. Accelerating experimental design by incorporating experimenter hunches. In *International Conference on Data Mining*, pp. 257–266, 2018.
- Mockus, J., Tiesis, V., and Zilinskas, A. The application of Bayesian methods for seeking the extremum. *Towards Global Optimization*, 2(117-129):2, 1978.
- Mosegaard, K. and Tarantola, A. Monte carlo sampling of solutions to inverse problems. *Journal of Geophysical Research: Solid Earth*, 100(B7):12431–12447, 1995.
- Nguyen, V. and Osborne, M. A. Knowing the what but not the where in Bayesian optimization. In *International Conference on Machine Learning*, pp. 7317–7326, 2020.
- Nguyen, V., Gupta, S., Rana, S., Thai, M., Li, C., and Venkatesh, S. Efficient Bayesian optimization for uncertainty reduction over perceived optima locations. In *International Conference on Data Mining*, 2019.
- Parker-Holder, J., Nguyen, V., and Roberts, S. J. Provably efficient online hyperparameter optimization with population-based bandits. *Advances in Neural Information Processing Systems*, 2020.
- Perrone, V., Shen, H., Seeger, M. W., Archambeau, C., and Jenatton, R. Learning search spaces for Bayesian optimization: Another view of hyperparameter transfer learning. In *Advances in Neural Information Processing Systems*, pp. 12771–12781, 2019.
- Popoviciu, T. Sur les équations algébriques ayant toutes leurs racines réelles. *Mathematica*, 9:129–145, 1935.
- Rahimi, A. and Recht, B. Random features for large-scale kernel machines. In Advances in Neural Information Processing Systems, pp. 1177–1184, 2007.
- Rasmussen, C. E. and Williams, C. K. I. *Gaussian Processes* for Machine Learning. MIT Prees, 2006.

- Richardson, R. R., Osborne, M. A., and Howey, D. A. Gaussian process regression for forecasting battery state of health. *Journal of Power Sources*, 357:209–219, 2017.
- Riihimäki, J. and Vehtari, A. Gaussian processes with monotonicity information. In *International Conference on Artificial Intelligence and Statistics*, pp. 645–652, 2010.
- Russo, D. J., Van Roy, B., Kazerouni, A., Osband, I., and Wen, Z. A tutorial on Thompsonsampling. *Foundations* and *Trends*® in *Machine Learning*, 11(1):1–96, 2018.
- Shahriari, B., Swersky, K., Wang, Z., Adams, R. P., and de Freitas, N. Taking the human out of the loop: A review of Bayesian optimization. *Proceedings of the IEEE*, 104 (1):148–175, 2016.
- Smola, A. and Vapnik, V. Support vector regression machines. Advances in Neural Information Processing Systems, 9:155–161, 1997.
- Srinivas, N., Krause, A., Kakade, S., and Seeger, M. Gaussian process optimization in the bandit setting: No regret and experimental design. In *International Conference on Machine Learning*, pp. 1015–1022, 2010.
- Thompson, W. R. On the likelihood that one unknown probability exceeds another in view of the evidence of two samples. *Biometrika*, 25(3/4):285–294, 1933.
- Wang, Z. and Jegelka, S. Max-value entropy search for efficient Bayesian optimization. In *International Conference* on *Machine Learning*, pp. 3627–3635, 2017.
- Wilson, J. T., Hutter, F., and Deisenroth, M. P. Maximizing acquisition functions for Bayesian optimization. In *Advances in Neural Information Processing Systems*, volume 31, pp. 9884–9895, 2018.
- Wilson, J. T., Borovitskiy, V., Terenin, A., Mostowsky, P., and Deisenroth, M. P. Efficiently sampling functions from Gaussian process posteriors. In *International Conference* on Machine Learning, pp. 10292–10302, 2020.
- Wilson, J. T., Borovitskiy, V., Terenin, A., Mostowsky, P., and Deisenroth, M. P. Pathwise conditioning of gaussian processes. *Journal of Machine Learning Research*, 22 (105):1–47, 2021.

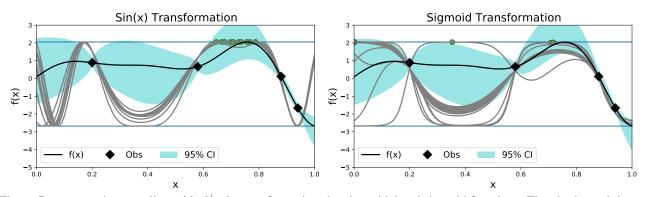


Figure 7: GP posterior sampling with f^+ , f^- transformations by sinusoidal and sigmoid functions. They both result in not good estimation although they satisfy the bounded constraints. The major issue with these transformations is that the GP samples are stretched out too much at the two tails f^+ and f^- .

A. Further Technical Details

A.1. Transformation by sinusoidal and sigmoid

We present two other ways to transform the GP posterior samples by incorporating the knowledge about f^+ and f^- . We utilize the sin wave and sigmoid transformations. For such transformations, we define a forward function to compute $f(\mathbf{x})$ given $h(\mathbf{x})$ which is constrained by either arcsin or log. Then, we define a reverse function to compute $h(\mathbf{x})$ given $f(\mathbf{x})$. These forward and reverse functions are summarized below:

• Using sinusoidal transformation: we define
$$\frac{f(\mathbf{x})-f^-}{f^+-f^-} = \frac{1}{2}\sin[h(\mathbf{x})] + \frac{1}{2}$$
 and $h(\mathbf{x}) = \arcsin\left\{2\left[\frac{f(\mathbf{x})-f^-}{f^+-f^-} - 0.5\right]\right\}$.

• Using sigmoid transformation: we define $\frac{f(\mathbf{x})-f^-}{f^+-f^-} = \frac{1}{1+\exp(-h(\mathbf{x}))}$ and $h(\mathbf{x}) = \log \frac{f(\mathbf{x})-f^-}{f^+-f^-}$.

Given f^+ and f^- , we transform the output **y** from the original space of $f(\cdot)$ to the space of $h(\cdot)$ as $h(\mathbf{x}) = \arcsin\left\{2\left[\frac{f(\mathbf{x})-f^-}{f^+-f^-}-0.5\right]\right\}$ for sinusoidal and $h(\mathbf{x}) = \log\frac{f(\mathbf{x})-f^-}{f^+-f^-}$ for sigmoid, respectively. We then draw samples from GP posterior of $h(\cdot)$ given $\{\mathbf{x}_i, h(\mathbf{x}_i)\}_{i=1}^N$. Next, we transform these samples back to the original space of $f(\cdot)$.

We note that sinusoidal and sigmoid transformations *require* the knowledge about both f^+ and f^- while square-root transformations and the proposed weighting strategy are more *flexible* to utilize either of f^+ , f^- or both of them.

We visualize the GP samples by using sinusoidal and sigmoid functions in Fig. 7. However, we note that such transformations will not result in promising samples as we have encoded the periodicity by sin wave or being stretched out by the sigmoid curve. These additional results justify our choice of squared-root transformation and weighting using f^+ and f^- in Section 3.1. We have also presented an empirical comparison in Fig. 3.

A.2. Implementation and Computational Complexity

We discuss the implementation aspect of our acquisition function, defined in Eq. (9) which involves sampling M GP posterior samples $g_1, ..., g_M$. The cost for this sampling is similar to that of Wilson et al. (2020).

The Gaussian likelihood $\pi(g_m)$ is computed for each GP sample $g_m(\cdot)$ once. We then optimize the acquisition function $\alpha^{\text{BES}}(\mathbf{x})$ by iteratively evaluating it at test points \mathbf{x} . The evaluation from the GP posterior sample is cheap, thanks to the scalability of GP posterior sampling using Matheron's rule that goes linearly with the number of test points (Wilson et al., 2020; 2021).

In particular, the computation of Eq. (9) reduces to Eqs. (10,11) for which we need to compute the GP posterior predictive mean $\mu(\mathbf{x}_m^+)$ and variance $\sigma^2(\mathbf{x}_m^+)$ in Eqs. (6, 7) with and without the presence of the considered location \mathbf{x} .

Note that in computing Eq. (10), we need to efficiently estimate the variance at \mathbf{x}_m^+ with the inclusion of \mathbf{x} , i.e., $\sigma_{\mathbf{x}}^2(\mathbf{x}_m^+)$.

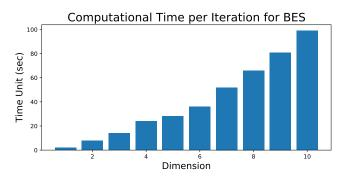


Figure 8: The computational cost for BES increases with dimension. Given an expensive black-box function $f(\cdot)$ which can take hours for evaluation, our computational time is reasonable within less than two minutes for 10 dimensions. The experiments are running on the Intel Core i7, 64GB Ram.

This can be efficiently computed by using the Block-wise matrix inversion lemma

$$K_{\mathbf{X}\cup\mathbf{x},\mathbf{X}\cup\mathbf{x}}^{-1} = \begin{bmatrix} K^{-1} & 0\\ 0 & 0 \end{bmatrix} + \underbrace{\frac{1}{\underbrace{k_{\mathbf{x},\mathbf{x}} - k_{\mathbf{x},\mathbf{X}}K_{\mathbf{X},\mathbf{X}}^{-1}k_{\mathbf{x},\mathbf{X}}^{T}}_{\sigma^{2}(\mathbf{x})}}_{\sigma^{2}(\mathbf{x})} \begin{bmatrix} K^{-1}\mathbf{k}_{\mathbf{x},\mathbf{X}}^{T}\mathbf{k}_{\mathbf{x},\mathbf{X}}K^{-1} & -K^{-1}\mathbf{k}_{\mathbf{x},\mathbf{X}}^{T} \\ -\mathbf{k}_{\mathbf{x},\mathbf{X}}K^{-1} & 1 \end{bmatrix}.$$
 (12)

Particularly, we decompose the inverse covariance matrix of $K_{\mathbf{X}\cup\mathbf{x},\mathbf{X}\cup\mathbf{x}}^{-1}$ given K^{-1} which is precomputed from the previous iteration. We then compute the remaining terms in the right handside using matrix multiplication to update $K_{\mathbf{X}\cup\mathbf{x}}^{-1}$.

We report the time taken for computing BES per iteration in Fig. 8. We can see that the computational cost for BES increases with dimension. This is because the number of time required to evaluate the acquisition function will grow with dimension. Nevertheless, the overall cost for suggesting a point is still less than two minutes for d = 10 while the black-box evaluation time is significantly higher, such as it takes a few hours to train a deep learning model.

A.3. Tightening the variances

To put things in context, the base distribution p_{base} for drawing GP posterior samples in Eq. (3) can be used as (i) standard GP (Wilson et al., 2020), (ii) weighting using GP (presented in Section 3.2) or (iii) weighting using SRGP (Section 3.3), respectively. We denote these approaches as p_{GP} , $p_{\text{w-GP}}$ and $p_{\text{w-SRGP}}$. We characterize the sample variance of the proposed approach and show that our strategy in weighting the GP posterior samples will tighten the variance of the GP samples considering in the 2*d* space formed shown in Fig. 2 (left). We adapt the Popoviciu's-inequality (Popoviciu, 1935) to bound the variance in our two dimensional space considered in Fig. 2 (left).

Lemma 3. Let $l \in \mathbb{R}^2$ be a random variable restricted to $[L_1, U_1]$ in the 1st dimension and $[L_2, U_2]$ in the 2nd dimension, we bound the variance of l as $\operatorname{Var}[l_1] \leq \frac{(U_1 - L_1)^2}{4}$ and $\operatorname{Var}[l_2] \leq \frac{(U_2 - L_2)^2}{4}$.

Proof. Let us denote $[L_1, L_2] = \inf l$ and $[U_1, U_2] = \sup l$. We define a function h by $h(t) = \mathbb{E}\left[(l-t)^2\right]$ that h'' > 0.

Computing the derivative h', and solving $h'(t) = -2\mathbb{E}[l] + 2t = 0$, we find that g achieves its minimum at $t = \mathbb{E}[l]$. We then consider the value of the function h at the specific point $t = \left\lceil \frac{U_1 + L_1}{2}, \frac{U_2 + L_2}{2} \right\rceil$. Next, we derive in the first dimension that

$$\begin{aligned} \operatorname{Var}[l_1] &= h\left(\mathbb{E}[l_1]\right) \le h\left(\frac{U_1 + L_1}{2}\right) \\ &= \mathbb{E}\left[\left(l_1 - \frac{U_1 + L_1}{2}\right)^2\right] & \text{by the definition of } h() \\ &= \frac{1}{4}\mathbb{E}\left[\left((l_1 - L_1) + (l_1 - U_1)\right)^2\right] \\ &\le \frac{1}{4}\mathbb{E}\left[\left(U_1 - L_1\right)^2\right] = \frac{\left(U_1 - L_1\right)^2}{4}. \end{aligned}$$

In the last inequality, we have $((l_1 - L_1) + (l_1 - U_1))^2 \le ((l_1 - L_1) - (l_1 - U_1))^2 = (U_1 - L_1)^2$ due to $l_1 - L_1 \ge 0$ and $l_1 - U_1 \le 0$. Similarly, we have the term in the second dimension bounded $\operatorname{Var}[l_2] \le \frac{(U_2 - L_2)^2}{4}$. This concludes our proof. \Box

Lemma 4. (Lemma 1 in the main paper) In the 2d space formed by $[f^+, f^-]$ and the GP posterior samples $\{g_m^+, g_m^-\}_{m=1}^M$, the sample variances by weighting our SRGP and GP are smaller than the GP posterior sampling (Wilson et al., 2020) making no use of the bounds: $Var[p_{W-GP}] \leq Var[p_{GP}]$ and $Var[p_{W-SRGP}] \leq Var[p_{GP}]$.

Proof. We first bound the sample variance in each dimension $d = \{1,2\}$ in Lemma 3 as

$$\operatorname{Var}\left[p_{\mathrm{GP}}^{(d)}\right] \leq \frac{\left(U_{\mathrm{GP}}^{(d)} - L_{\mathrm{GP}}^{(d)}\right)^2}{4}, \qquad \qquad \operatorname{Var}\left[p_{\mathrm{w-GP}}^{(d)}\right] \leq \frac{\left(U_{\mathrm{w-GP}}^{(d)} - L_{\mathrm{w-GP}}^{(d)}\right)^2}{4}$$

where the base distribution can be used as (i) a standard GP, i.e., $p_{\text{GP}} = p(f(\cdot) | \mathbf{X}, \mathbf{y})$ or (ii) a weighted GP with the bounds information $p_{\text{w-GP}} := \pi(g_m) = p(f(\cdot) | \mathbf{X}, \mathbf{y}, f^+, f^-)$.

In our GP sampling and weighting setting, we have $U_{w-GP}^{(d)} < U_{GP}^{(d)}, \forall d = 1, 2 \text{ and } L_{w-GP}^{(d)} > L_{GP}^{(d)}, \forall d$. This means $U_{w-GP}^{(d)} - L_{w-GP}^{(d)} \le U_{GP}^{(d)} - L_{GP}^{(d)}, \forall d$ and thus $\operatorname{Var}[p_{w-GP}] \le \operatorname{Var}[p_{GP}]$. Using similar derivations, we get $\operatorname{Var}[p_{GP}] \ge \operatorname{Var}[p_{w-SRGP}]$, thus conclude the proof.

This can also be seen in Fig. 2 that indeed $\pi(g_m)$ is bounded by the density of p_{GP} . Using SRGP, we have flexibly transformed the surrogate toward the desirable area. Under such transformation, the p_{w-SRGP} has a tighter upper bound than p_{w-GP} . We next show that the sample variance of the base distribution using weighting SRGP is smaller than using weighting GP, $\operatorname{Var}[p_{w-SRGP}] \leq \operatorname{Var}[p_{w-GP}]$. Thus, the SRGP is more sample-efficient than GP in generating accepted samples. This variance property can be intuitively seen from Fig. 2 (left) in the main paper. In addition, we have numerically demonstrated this comparison in Table 1.

Lemma 5. (Lemma 2 in the main paper) In the 2d space formed by $[f^+, f^-]$ and the GP posterior samples $\{g_m^+, g_m^-\}_{m=1}^M$, the sample variance of weighting SRGP is smaller than weighting GP: $Var[p_{w-SRGP}] \leq Var[p_{w-GP}]$.

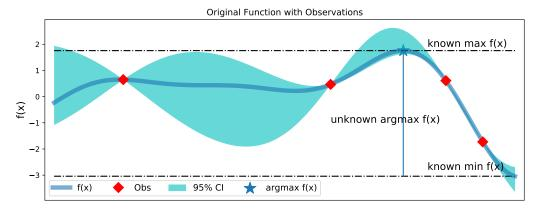
Proof. To prove $\operatorname{Var}[p_{W-SRGP}] \leq \operatorname{Var}[p_{W-GP}]$, it is equivalent to show that the inequality is true in all dimensions of the distributions considered. Let us denote the first dimension (1) is formed by $f^+ - \max g_m(\cdot)$ and the second dimension (2) is by $f^- - \min g_m(\cdot)$, see Fig. 2. In the first dimension, we have the upper bound $U_{W-SRGP}^{(1)} = f^+ + 2\eta_+ \leq U_{W-GP}^{(1)}$, the equality happens when $\eta_+ \to \infty$ and the lower bound $L_{W-GP}^{(1)} = L_{W-SRGP}^{(1)}$. In the second dimension, we have both the upper and lower bounds unchanged $U_{W-GP}^{(2)} = U_{W-SRGP}^{(2)}$ and $L_{W-GP}^{(2)} = L_{W-SRGP}^{(2)}$.

Using Lemma 3, we conclude that $\operatorname{Var}\left[p_{w-\operatorname{SRGP}}^{(1)}\right] \leq \operatorname{Var}\left[p_{w-\operatorname{GP}}^{(2)}\right]$ and $\operatorname{Var}\left[p_{w-\operatorname{SRGP}}^{(2)}\right] \leq \operatorname{Var}\left[p_{w-\operatorname{GP}}^{(2)}\right]$. In words, the base distribution by SRGP (Section 3.3) $p_{w-\operatorname{SRGP}}$ has a tighter sample variance than $p_{w-\operatorname{GP}}$ (Wilson et al., 2020).

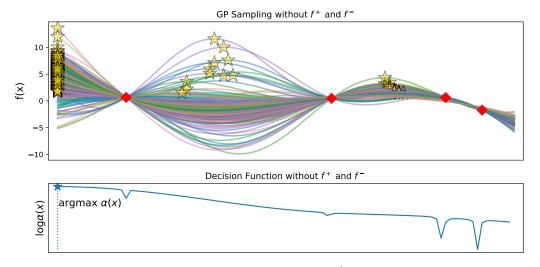
A.4. Decoupling Approach for GP Posterior Sampling

The central idea of decoupled sampling relies on the Matheron's rule for Gaussian random variables (Journel & Huijbregts, 1978; Chiles & Delfiner, 2009; Doucet, 2010) that uses variational Fourier features for an approximate prior and a deterministic data-dependent update term to efficiently draw samples. Let $\phi(\mathbf{x}_i) = \sqrt{\frac{2}{l}} \cos(\theta_i^T \mathbf{x}_i + \tau_i)$, where θ_i is sampled proportional to the kernel's spectral density, $\tau_i \sim \mathbb{U}(0, 2\pi)$ and l is the random feature dimension. We draw samples $f_* | \mathbf{X}, \mathbf{y}, \mathbf{x}_*, \omega_m$ from a GP posterior and evaluate them at any test input $\mathbf{x}_* \in \mathcal{X}$ as

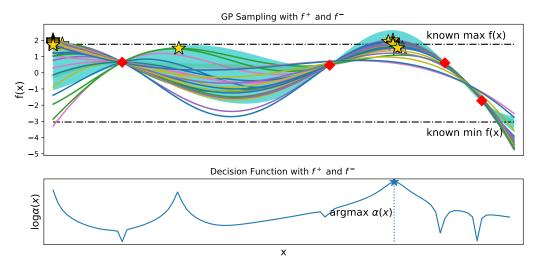
$$g_m(\mathbf{x}_*) = \sum_{i=1}^{l} \underbrace{w_i \phi_i(\mathbf{x}_*)}_{\text{random}} + \sum_{j=1}^{N} \underbrace{v_j k(\mathbf{x}_*, \mathbf{x}_j)}_{\text{deterministic update}}$$
(13)



(a) We have a black-box function $f(\mathbf{x})$ including four observations (red dots), the maximum value f^- and minimum value f^- . The goal is to find the unknown maximum location $\arg \max f(\mathbf{x})$.



(b) *Top*: GP posterior sampling p_{base} without the knowledge about f^+ and f^- . *Bottom*: the decision function will select the left corner which is not the correct maximum location.



(c) *Top*: GP posterior sampling $\pi(g_m)$ guided by the f^+ and f^- . *Bottom*: our decision selects the next point for evaluation correctly as the unknown maximum location, i.e., $\arg \max \alpha^{\text{BES}}(\mathbf{x}) = \arg \max f(\mathbf{x})$.

Figure 9: Illustrating the BES. *Top*: a black-box function $f(\mathbf{x})$ and four observations (red dots). Middle: p_{base} as a GP and the decision without the weighting $\pi(g_m)$. *Bottom*: p_{base} as a SRGP and the decision with the weighting $\pi(g_m)$.

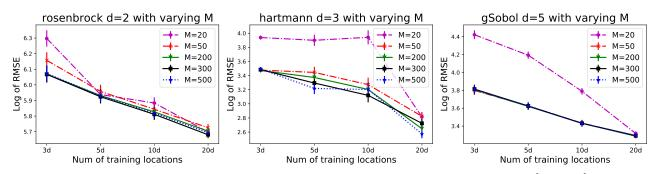


Figure 10: GP posterior sampling with different number of GP samples *M*. Our approach using $M \in [200, 500]$ will result in the best performance while M = 20 is the worst.

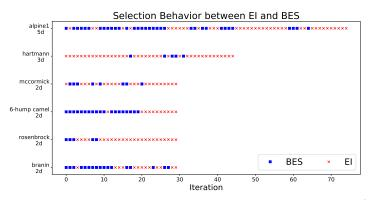


Figure 11: When none of the GP sample is accepted (falling into the two standard deviation of $\pi(g_m)$), we propose to use the EI instead of BES. This illustration indicates the switching behavior between EI vs BES.

where $w_i \stackrel{\text{iid}}{\sim} \mathcal{N}(0,1)$, $\mathbf{w} = [w_i, ..., w_l]^T \in \mathbb{R}^l$, $\Phi = \phi(\mathbf{X}) \in \mathbb{R}^{N \times l}$ and $v = (K + \sigma_f^2 \mathbf{I})^{-1} (\mathbf{y} - \Phi \mathbf{w})$. The sampling process above relies on the randomness of the Fourier features (Rahimi & Recht, 2007) via $\omega_m \sim p(\omega)$

$$\mathbb{E}_{p(\boldsymbol{\omega})}\left[f_* \mid \mathbf{X}, \mathbf{y}, \boldsymbol{\omega}\right] \approx \frac{1}{M} \sum_{\boldsymbol{\omega}_m \sim p(\boldsymbol{\omega})} g(. \mid \mathbf{X}, \mathbf{y}, \boldsymbol{\omega}_m)$$
(14)

where $\omega_m = \{\theta_m, \tau_m\}.$

B. Illustration of Bounded Entropy Search (BES) Decision Function

We first illustrate the decision function of BES given the knowledge of $f^+ = \max f(\mathbf{x}) + \mathcal{N}(0, \eta_+^2)$ and $f^- = \min f(\mathbf{x}) + \mathcal{N}(0, \eta_-^2)$ in Fig. 9. Given limited observations in Fig. 9a, it may be difficult to infer the unknown optimum location arg max $f(\mathbf{x})$. However, we can utilize the information about the upper bound and lower bound to better identify this location of interest. In particular, we show that incorporating f^+ and f^- can help to identify correctly the unknown maximum location in Fig. 9c while we may fail without such extra knowledge as shown in Fig. 9b.

C. Ablation Studies

C.1. Ablation studies with different number of GP samples M

We study the sensitivity with varying the number of GP samples $M \in [20, 50, 200, 300, 500]$ in Fig. 10. We show that if the number of *M* is set too small, such as $M \le 50$. The performance can be negatively affected. On the other hand, if we set *M* large enough to be [200, 500], they tend to perform similarly well. This is the recommended range for *M* in our paper. We also note that increasing *M* will require more computation. However, such computation can be well handled by using parallel infrastructure since drawing GP samples are independent from each other.

C.2. Switching between EI vs BES

We have discussed in Section 6 that there will be some iterations when we don't have any accepted sample for BES. There are several reasons, such as the observations are biased to reconstruct the black-box function, the estimated GP hyperparameters are not correct. When the number of accepted sample is zero, we will perform Expected improvement (Jones et al., 1998) instead of BES. Our choice is motivated by the strong and robust performance of EI. We note that an alternative solution is to keep sampling the GP until we get at least one accepted sample.

We illustrate this behavior in Fig. 11. We use the number of GP samples M = 200, $\eta_+^2 = 0.03d$ and $\eta_-^2 = 0.6d$ where d is the input dimension. We use a blue square to indicate if BES is used for this iteration and red cross if EI is taken.

C.3. Sensitivity analysis of misspecifying f^+ and f^- for GP posterior sampling

We study the sensitivity to the GP posterior sampling performance by misspecifying the upper and lower bounds. In the benchmark function considered, we know the true max $f(\mathbf{x})$ and min $f(\mathbf{x})$ in advance. We make use of these optimum values and vary the misspecified levels $\eta_+^2 = \eta_-^2 \in [0, 1, 3, 5]$ for which $f^+ = \max f(\mathbf{x}) + \mathcal{N}(0, \eta_+^2)$ and $f^- = \min f(\mathbf{x}) + \mathcal{N}(0, \eta_-^2)$. This level is considered in a standardized output space $y \sim \mathcal{N}(0, 1)$. We present the result in Fig. 12. It is expected that increasing the misspecified levels will lead to degrading the performance. However, our model still performs better than the vanilla GP sampling (Wilson et al., 2020) in most cases. Especially, when we have limited observations of less than 5*d* training locations, our model outperforms GP sampling when $\eta^2 \leq 3$.

Relaxing this misspecify level $\eta \to \infty$ will let the performance of w-GP at least reduce to the case of Wilson et al. (2020) while the performance of w-SRGP will be more sensitive as the transformation depends on η_+ .

C.4. BES without weighting

We provide another set of experiments to compare the performance with a variant version of BES without weighting and Thompson sampling (or BES with M = 1). The BES setting without weighting is when we ignore the f^+ , f^- and set the weighting probability $\pi(g_m) = \frac{1}{M}$ uniformly.

The result in Fig. 13 shows that BES without weighting (blue curve) will perform poorly. Particularly, this version will accept all GP posterior samples and gain information about all of them, including the 'bad' samples. Thompson sampling (TS) is a special version of BES in which we only draw a single GP posterior sample $g(\cdot)$. Then, we select a next point to evaluate as the mode of this sample, i.e., $\mathbf{x}_t = \arg \max_{\mathbf{x} \in \mathscr{X}} g(\mathbf{x})$. Because drawing a single GP sample will have very high variance especially in high-dimension, TS will generally perform inferior in a sequential BO setting, as discussed in Hernández-Lobato et al. (2014); Nguyen et al. (2019).

Exploiting the knowledge about both f^+ , f^- will result in better performance than exploiting a single value of f^+ . Especially, our BES version using square-root transformation GP will achieve the best performance. This is because it can take into account the knowledge of f^+ to tailor the GP sample toward the desirable shape. This will lead to better theoretical property as presented in Lemma 1 and Lemma 2.

The result in this experiment again highlights our choice of BES in Section 4 that gains information only about good GP posterior samples.

D. Experimental evaluation

D.1. Experimental setting

The benchmarks function and their ranges are available online.⁴ We summarize the hyperparameters and their min-max ranges used in the machine learning tuning experiments in Table 2.

• Support vector regression (Smola & Vapnik, 1997) on Abalone dataset. The Abalone dataset is available publicly.⁵ We specify the upper bound as $f^+ = -1.92$ and do not set the lower bound.

⁴https://www.sfu.ca/~ssurjano/optimization.html

⁵https://archive.ics.uci.edu/ml/datasets/abalone

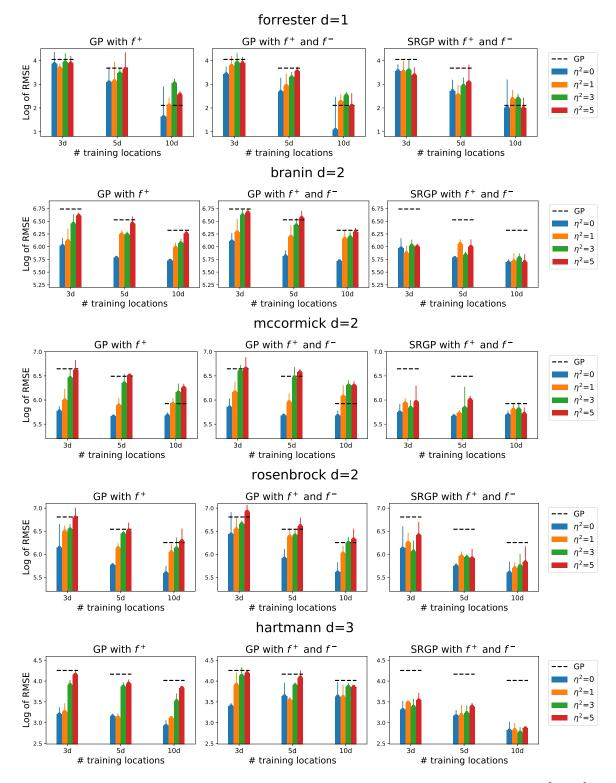


Figure 12: We study the sensitivity of the model by misspecifying the f^+ and f^- with different levels $\eta^2 := \eta_+^2 = \eta_-^2 \in [0, 1, 3, 5]$. Increasing the misspecified levels will degrade the performance. It is important to note that our w-GP with misspecification still performs better than the vanilla GP sampling (Wilson et al., 2020) which does not use the bounds, especially when the number of training locations is small, 3*d* or 5*d*. Asymptotically, when $\eta \to \infty$, our w-GP will accept all samples and become the case of Wilson et al. (2020).

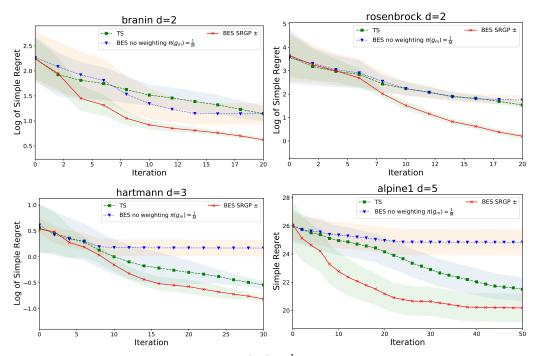


Figure 13: Ablation studies of BES without weighting or $\pi(g_m) = \frac{1}{M}$. The weighting step significantly boosts the performance of BES to achieve significantly better than BES without weighting (blue curve).

Table 2: The ranges for each hyperparameter used for tuning machine learning algorithms.

XGBOO	ST								
Variables	Min	Max	CN	CNN			Support vector regression		
min_child_weight	1	20	Variables	Min	Max		Variables	Min	Max
colsample_bytree max_depth	0.1 5	1 15	batch size	16	100		C	0.1	1000
subsample	0.5 0	1 10	learning rate max iteration	$1e^{-6}$ 5	$1e^{-2}$ 50		epsilon gamma	$1e^{-6}$ $1e^{-6}$	5
alpha	0	10							

- XGBOOST classification (Chen & Guestrin, 2016): we use Pima Indians Diabetes database.⁶ We set the bounds $f^+ = 0.75$, $f^- = 0.65$ for the result presented in Fig. 4. Then, we vary the upper bound $f^+ \in [0.7, 0.73, 0.75, 0.77, 0.8, 0.9]$ to study the sensitivity with different choices of f^+ presented in Fig. 6.
- CNN classification (LeCun & Bengio, 1995) on a subset (10%) of CIFAR10. We use the bounds of $f^+ = 61.5$ and $f^- = 0$.

D.2. Additional experiments

We present additional experiments for GP posterior sampling in Fig. 14 and Bayesian optimization in Fig. 15. The additional results are consistent with the results presented in the main paper. $BES\pm$ (exploiting both f^+ and f^-) achieves the best performance.

⁶https://www.kaggle.com/uciml/pima-indians-diabetes-database

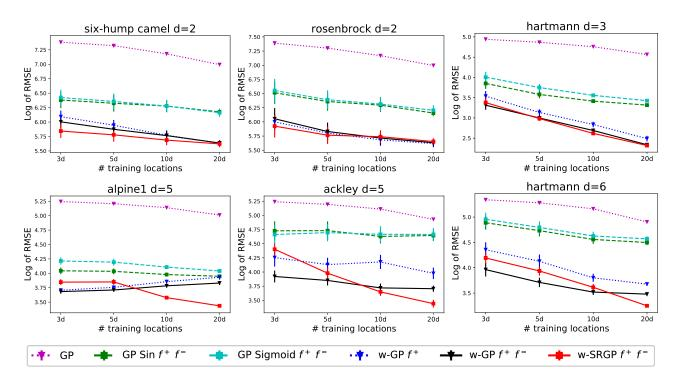


Figure 14: We measure the root mean squared error (RMSE) loss from M = 200 GP samples $g(\cdot)$ against the true function $f(\cdot)$ with different number of training points [3d, 5d, 10d, 20d] where d is the number of input dimensions. The f^+ and f^- are known from the black-box function. The overall trends indicate that (i) the loss is smaller with increasing number of training points and (ii) exploiting the external knowledge about f^+ and f^- will lead to better estimation than exploiting f^+ alone. When we get sufficient observations, e.g., the number of training locations is 20d, the performance of w-GP f^+, f^- resembles w-SRGP f^+, f^- . The error bar is estimated over 30 independent runs.

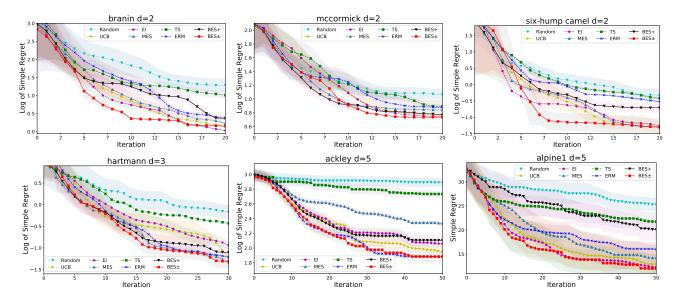


Figure 15: We present additional results for Bayesian optimization using benchmark functions. Our BES \pm (using both f^+, f^-) achieves better performance than BES \pm (using f^+ alone) and ERM (using f^+ alone) (Nguyen & Osborne, 2020).